ARMY RESEARCH LABORATORY

Modeling Impacts for Cold-Gas Dynamic Spray

by William S. de Rosset

ARL-TR-3890 **September 2006**

NOTICES

Disclaimers

The findings in this report are not to be construed as an official Department of the Army position unless so designated by other authorized documents.

Citation of manufacturer's or trade names does not constitute an official endorsement or approval of the use thereof.

Destroy this report when it is no longer needed. Do not return it to the originator.

Army Research Laboratory
Aberdeen Proving Ground, MD 21005-5069

ARL-TR-3890 **September 2006**

Modeling Impacts for Cold-Gas Dynamic Spray

William S. de Rosset
Weapons and Materials Research Directorate, ARL

REPORT DOCUMENTATION PAGE

Form Approved
OMB No. 0704-0188

1. REPORT DATE *(DD-MM-YYYY)*	2. REPORT TYPE	3. DATES COVERED (From - To)
September 2006	Final	July 2005–March 2006

4. TITLE AND SUBTITLE
Modeling Impacts for Cold-Gas Dynamic Spray

5a. CONTRACT NUMBER

5b. GRANT NUMBER

5c. PROGRAM ELEMENT NUMBER

6. AUTHOR(S)
William S. de Rosset

5d. PROJECT NUMBER
AH84

5e. TASK NUMBER

5f. WORK UNIT NUMBER

7. PERFORMING ORGANIZATION NAME(S) AND ADDRESS(ES)
U.S. Army Research Laboratory
ATTN: AMSRD-ARL-WM-MB
Aberdeen Proving Ground, MD 21005-5069

8. PERFORMING ORGANIZATION REPORT NUMBER
ARL-TR-3890

9. SPONSORING/MONITORING AGENCY NAME(S) AND ADDRESS(ES)

10. SPONSOR/MONITOR'S ACRONYM(S)

11. SPONSOR/MONITOR'S REPORT NUMBER(S)

12. DISTRIBUTION/AVAILABILITY STATEMENT
Approved for public release; distribution is unlimited.

13. SUPPLEMENTARY NOTES

14. ABSTRACT
A one-dimensional penetration model has been developed to analyze the cold-gas dynamic spray process in hopes of establishing a constant minimum normalized penetration depth for particle adhesion. The simple model was in disagreement with results extrapolated from published copper-on-steel impact data. Possible reasons for the disagreement are discussed. A possible bonding mechanism is proposed that is dependent on the flow properties of both the particle and substrate.

15. SUBJECT TERMS
cold-gas dynamic spray, particle penetration mechanics, particle adhesion

16. SECURITY CLASSIFICATION OF:			17. LIMITATION OF ABSTRACT	18. NUMBER OF PAGES	19a. NAME OF RESPONSIBLE PERSON
a. REPORT	b. ABSTRACT	c. THIS PAGE			William S. de Rosset
UNCLASSIFIED	UNCLASSIFIED	UNCLASSIFIED	UL	32	19b. TELEPHONE NUMBER (*Include area code*) 410-306-0816

Contents

List of Figures

Acknowledgments

The author would like to acknowledge the help of Constantine Fountzoulas, who ran several Autodyne calculations, and Marc Pepi, who polished and etched the sample of stainless steel. Mr. Pepi also made the hardness measurements on the sample. Special thanks go also to Dr. Steven Segletes for pointing out the inherent strain rate effects in the cold spray process and for his helpful comments on the modeling effort.

INTENTIONALLY LEFT BLANK.

1. Introduction

Ever since Supersonic Particle Deposition (SPD), otherwise known as cold-gas dynamic spray, showed the promise of being able to coat substrates with a variety of materials, there has been speculation as to how the bond is formed between the impacting particle and the substrate. Most of the successful spray depositions have occurred for metal particles impacting metal surfaces, which has led some authors to suppose that an oxide surface layer must be broken before bonding will occur (*1*). The fact that there is a minimum particle impact velocity required for particle adhesion is consistent with this hypothesis. Others have seen a correlation between impact velocities and calculated values of the onset of adiabatic shear instability in the particle (*2*, *3*). The bonding mechanism invoked in this case is that the adiabatic shear occurs at and welds the contacting surfaces. In some instances, the penetration of the particle is deep enough to provide a mechanical rivet of the particle to the substrate (*4*). Another supposition is that a jet is formed between the spherical particle and the substrate, similar to that formed in explosive bonding (*1*–*3*). The jet acts to clean the substrate surface of any oxide layer.

Clearly, a particle will adhere to a metal substrate if the impact velocity is high enough to supply a mechanical bond produced by deep penetration of the target. (Of course, the velocity cannot be so high as to vaporize the particle.) What is more interesting is the nature of the bonding process at the lowest velocity at which a particle will stick to the substrate. A minimum particle impact velocity for adhesion indicates that there is a minimum value of the penetration depth for any particle-substrate material combination. From the data in the literature a normalized penetration depth, defined here as the penetration depth divided by the particle radius, can be determined. If the value of the normalized penetration depth were the same for all material combinations, then some insight might be gained on the nature of the bond between the particle and substrate.

Unfortunately, there is very little information available on penetration depths at the onset of adhesion. The approach taken here was to develop a simple predictive model and use available data to test its accuracy. The model would then be used to predict the penetration depths at reported minimum impact velocities for other material combinations. Section 2 describes a particular experiment that contains an extensive amount of impact data for one particular material combination, copper and stainless steel. With several reasonable assumptions, the normalized penetration depth is determined. Section 3 contains the development of a one-dimensional impact model used to predict depth of penetration. The model is found to deviate from the observed results. In section 4, possible reasons for the discrepancy are discussed and sensitivity analyses are conducted to determine the impact of certain input parameter changes. Section 5 offers some general observations on the incipient bonding process and suggests that mechanical bonding is possible even for low-velocity impacts. Section 6 provides a summary of the report.

2. Data Analysis

In order to interpret SPD experimental data correctly, one must understand the statistics behind the process. First, the particles that are used in the process are not a single size but come in a distribution with a mean size and a variance. In most cases, the distribution is normal (Gaussian), but this may not always be the case. The distribution of particle sizes leads to a distribution of particle velocities for any particular set of operating parameters (e.g., gas pressure, gas type, nozzle design, temperature, and nozzle-to-target distance) used with the SPD equipment. Aerodynamic considerations and certain approximations lead to the simple relationship between a particle's mass and its velocity:

$$V_p = V(m_o/m)^{1/2}, \quad (1)$$

where V_p is the particle velocity, V is the average particle velocity, m is the particle mass, and m_o is the average particle mass (*5*). In general, the smaller particles have a higher velocity than the mean, and the larger particles have a smaller velocity than the mean. It has been found that there is not good quantitative agreement between this simple formula and experimental data for copper and aluminum particles (*6*), although the overall trend is correct. In addition, the velocity of a given size particle will decrease the farther it is from the center of the gas stream.

Dykhuizen et al. (*1*) conducted a series of experiments in which they sprayed copper particles on a 304 stainless steel substrate and measured both the crater volume and the particle volume of those particles that stuck. The copper powder had a mean particle diameter of 22 μm, with a 5.6-μm standard deviation. Four average particle velocities were chosen, and the actual velocities achieved were 403, 521, 606, and 704 m/s.

Figure 1 shows the data for the 521 m/s data set. A straight line has been added to the data. All but one of the data points fall above the line. The particle sizes fall between 10 and 30 μm in diameter, with more of the data points clustered at the lower end of the range. (The volume corresponding to a 22-μm-sized particle is 5575 μm^3.) The main conclusion to be drawn from these data points is that regardless of the particle size, there is a minimum crater-volume-to-particle-volume (CV/PV) ratio. The particular line drawn in figure 1 gives CV/PV as 0.058. (There is one outlier below the line at a particle volume of about 7500 μm^3 which is neglected in this analysis.) Similar data for an impact velocity of 606 m/s is also presented in Dykhuizen et al. (*1*). All but one of the 68 data points in this set have CV/PV greater than 0.06.

Both the experiments conducted at 521 and 606 m/s contained particles that had the necessary minimum velocity to stick to the target. For those particles with a CV/PV ratio greater than 0.06, it is assumed that they impact the target at a velocity that is higher than the minimum needed to stick. However, the same authors found that no copper particles stuck to the stainless steel at a 403 m/s impact velocity. Some of the smaller particles have an impact velocity in excess of this

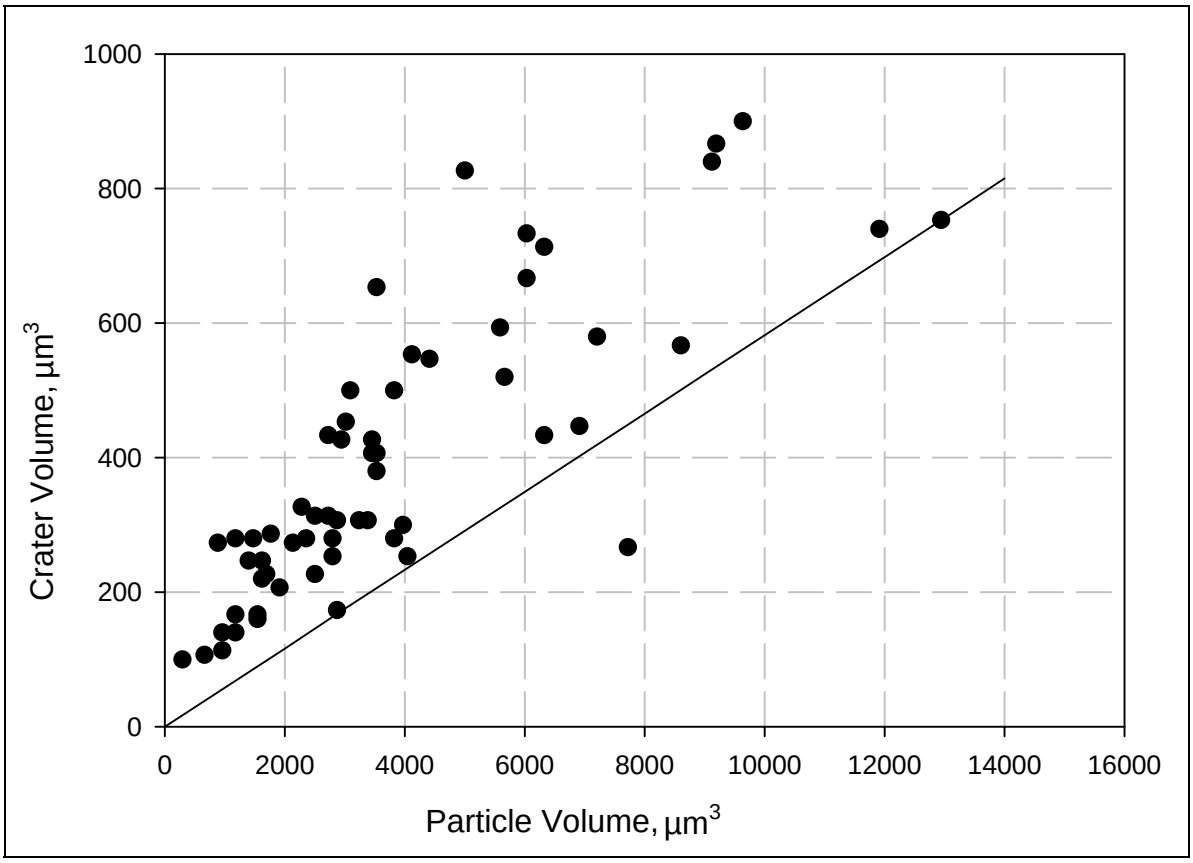

Figure 1. Crater volume vs. particle volume for copper particles impacting and sticking to stainless steel at an average velocity of 521 m/s (Dykhuizen et al. [*1*]).

value, so that the minimum impact velocity needed for sticking would certainly be higher than 403 m/s, but less than 521 m/s.

Some simple geometric considerations provide an estimate of the penetration depth to particle radius ratio for the particles that stuck to the target. First, we assume that the crater wall stays in contact with the particle over the complete extent of the crater and that the particle radius does not change significantly until the particle ceases its axial motion. This assumption appears to be reasonable based on the cross-section measurement of a particle that is sticking to the substrate shown in figure 8 of Dykhuizen et al. (*1*). (The model development in section 3 will allow the particle to deform, but most of the deformation occurs during the latter stages of the penetration process.) In this case, we have for $0 <= X <= R$

$$CV = 1/3\ \pi\ X^2\ (3R - X), \tag{2}$$

where X is the final penetration depth and R is the particle radius. The volume of a spherical particle is given by

$$PV = 4/3\ \pi\ R^3. \tag{3}$$

Setting CV/PV to the experimentally observed value (see figure 1) of 0.06 and solving for the value of X/R, we get

$$X/R = 0.298. \quad (4)$$

For a particle with a 22-μm diameter, the penetration depth would be 3.3 μm. This is a surprisingly shallow penetration depth, but it is consistent with figure 8 of Dykhuizen et al. (*1*), which shows a crater profile whose depth is a little over 2 μm.

3. Model Development

There exist many computer codes of various types (Eulerian, Lagrangian, smooth-particle hydrodynamic, etc.) that can easily be used to model the impact of a metal sphere onto a metal target. These codes employ very sophisticated constitutive relations and come with a fixed library of constants that are selected based on the type of constitutive relation chosen for the calculation. They are capable of solving complicated problems in three dimensions, if required, although the use of symmetry is used to reduce run time and memory requirements. The full dynamic process can be handled with stress wave propagation calculations and material failure evolution models. This high-powered computing comes with a cost, however. In many cases, it is difficult to determine which parameters are the most important in determining the outcome. It takes a skilled operator versed in the inner working of the code to differentiate computational artifacts (created, say, by the mesh size) from real effects. The output of data from a code run has become so large that we depend a great deal on scientific visualization to make sense of them. This leads to additional work to adjust the output presentation.

There also exist simple analytical approaches to impact problems. They have the advantage that anyone with a reasonable mathematics and scientific background can not only understand how the model works, including assumptions and limitations, but also be able to exercise the model. The approach taken with this work was to use a simple one-dimensional penetration model, adapted to a ball-on-plate geometry. The modeling was used as an aid to understanding low-impact-velocity phenomena, with the ultimate goal of understanding how particles first begin to adhere to surfaces.

The basis for the model is the classic Bernoulli equation, modified by Tate (*7*, *8*) and Alekseevskii (*9*):

$$\Sigma = \tfrac{1}{2} \rho_p (v - u)^2 + Y_p = \tfrac{1}{2} \rho_t u^2 + R_t . \quad (5)$$

Here, ρ_p and ρ_t are the particle and target densities, respectively, v is the speed of the rear of the particle, u is the penetration speed, Y_p is the strength of the particle, and R_t is the target resistance. Σ is the axial stress along the centerline of the particle. It will be assumed that the

particle is a sphere and that it penetrates as a rigid body. This is a reasonable assumption since the particle does not erode but maintains its mass throughout the penetration process. However, the assumption is inconsistent with the fact that the particle deforms. At some point, possibly late in the penetration process, the penetration will cease but there will still be a center-of-mass velocity. While this assumption will undoubtedly lead to some disagreement between the model calculations and observed results, it is made in order to move the analysis forward. The assumption dictates that v = u, and equation 1 reduces to

$$\Sigma = \tfrac{1}{2} \rho_t v^2 + R_t \, . \tag{6}$$

Since the penetration process occurs in three dimensions, some reasonable assumptions must be made to allow the one-dimensional model to agree with experimental results. The first assumption is that the retarding force on the particle is given by the axial stress times the projected contact area of the particle. The projected contact area is calculated from the circle formed by the intersection of the particle projected onto the original surface. The second assumption is that the target resistance is proportional to the target flow stress. That is,

$$R_t = \beta \, Y_t \, , \tag{7}$$

where β is the constant of proportionality and Y_t is the target flow stress.

The main problem then becomes one of finding a reasonable value for the proportionality constant. A one-dimensional model that incorporates plasticity theory has been developed by Goodier (*10*). He gives the retarding force (target resistance) as

$$F_r = q \, (2a)^n \, , \tag{8}$$

where n is generally taken as 2 and $q = 2.77 \, Y_t$. Given that

$$F_r = \pi \, a^2 \, R_t \, , \tag{9}$$

we get $\beta = 3.5$. Walker and Anderson (*11*) estimate the value of β from a penetration mechanics analysis involving the integration of momentum along the centerline of a penetrator and making certain reasonable assumptions about the velocity profiles in the target and penetrator materials:

$$\beta = 7/3 \ln(\alpha) \, , \tag{10}$$

where α is the extent of the plastic zone in the target material. These authors calculate the value of α for a rigid body penetrator to be

$$\alpha = (2E_t/3Y_t)^{1/3} \, , \tag{11}$$

where E_t is the elastic modulus of the target material. Using a yield strength of 215 MPa and a Young's modulus of 200 GPa for stainless steel, we get $\alpha = 8.5$ and $\beta = 5.0$. Of course, the particular example we are considering for the cold spray application is not rigid in the usual sense.

For static indentations, a rule of thumb is that the Brinnell hardness number in kg/mm^2 is three times the ultimate tensile strength of many steel alloys (*12*). If the Brinnell hardness can be considered a "target resistance," then $\beta = 3$.

These considerations point to the likelihood that the value of β lies in the range of 3 to 5. Rather than pick a value of β that fits the data, this range will be used to see how close the calculations come to the observed values.

Of even more concern is the value to be used as the target flow stress. Micrographs taken of a 304 stainless steel sample confirmed the supposition that the grain size diameter of this material can be much larger than the diameter of an individual particle. A representative micrograph is shown in figure 2.

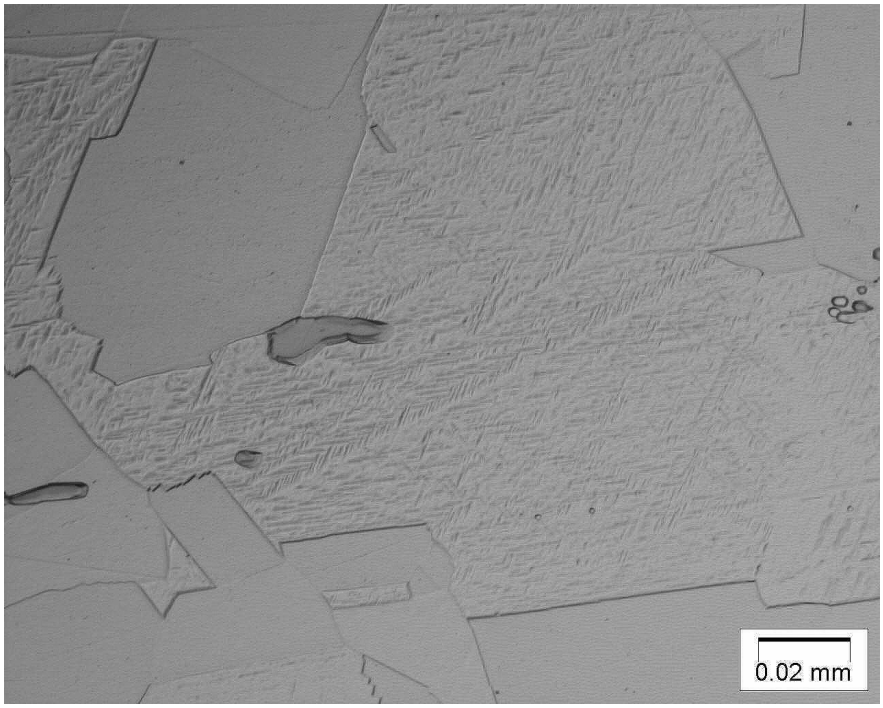

Figure 2. Surface of 304 stainless steel showing grain structure.

Grain size will depend, to a large extent, on the processing history of the material. The processing history of the material used by Dykhuizen et al. (*1*) is not known. Neither is the processing history of the material shown in figure 2 known. However, it is interesting to note that in the latter case, the craters made by several 20-μm particles could be totally enclosed in a single grain. (The length scale shown in the figure is 20 μm.) Since the experiments suggest that a particle penetrated only a third of its radius, the impact area would have a diameter less than 20 μm. This suggests that individual grain properties should be used in the calculations, rather than the bulk properties.

Figure 2 shows grains with two different appearances. One has a feathery appearance, and the other is more clear. Knoop microhardness measurements were made on both types of grains using a 50 gram-force load. The hardnesses were converted to tensile strength values and the results were 110 and 98 ksi for the strengths of the feathery and clear grains, respectively. In order to examine a single grain at a time, standard procedures were not followed. Consequently, the results must be considered approximate at best (*13*). Nevertheless, they indicate a strength level several times that of the bulk material (~30 ksi). For these calculations, the flow stress will be taken to be 700 MPa.

While the yield strength of the copper does not enter the calculation directly, it must be assumed that the strength of the copper is greater than the target resistance for there to be rigid body penetration. The yield strength of annealed copper is below 100 MPa (the room temperature yield strength used in the Johnson-Cook constitutive model is 90 MPa [*12*]). However, the copper particles are so small that they are most likely single crystals. Therefore, the strength of an individual particle may be much higher than that of the bulk material. In addition, the strain rates at which cold spray takes place are extremely high and can be estimated by dividing the impact velocity (500 m/s) by a typical dimension (for instance, the particle diameter, 20 μm). Thus, strain rates on the order of 10^7 s^{-1} or greater are produced during impact. These rates are far higher than even split-Hopkinson bar experiments can reach. The yield strength of the copper particles can be expected to increase with increasing strain rate, but the amount of increase is unknown. Finally, spherical-nosed (or simply spherical) penetrators are constrained by the crater they make in the target so that the penetrator material appears to be stronger than it actually is (*14*, *15*).

From geometric considerations, the projected contact area of the particle and the target, πa^2, is given by

$$\pi a^2 = \pi(Dx - x^2), \tag{12}$$

where D = 2R and x(t) is penetration depth as a function of time. When x = R, then the projected contact area is simply πR^2. The equation of motion then becomes

$$\begin{aligned} m dv/dt &= -(\tfrac{1}{2}\, \rho_t\, v^2 + R_t)\, \pi(Dx - x^2), \qquad 0 < x < R \\ &= -(\tfrac{1}{2}\, \rho_t\, v^2 + R_t)\, \pi R^2, \qquad x > R\,. \end{aligned} \tag{13}$$

The initial conditions are x(0) = 0 and v(0) = impact velocity. This equation is solved for x as a function of time through an iterative method using an Excel spreadsheet.* The appendix contains the details of these calculations. A time step of 0.2 ns was used; the results did not change significantly when a time step of 0.5 ns was used. Figure 3 shows the calculated penetration depth as a function of time for two values of β. The final penetration depths are 10.0 and 7.67 μm for

*Excel is a registered trademark of the Microsoft Corporation (Redmond, WA).

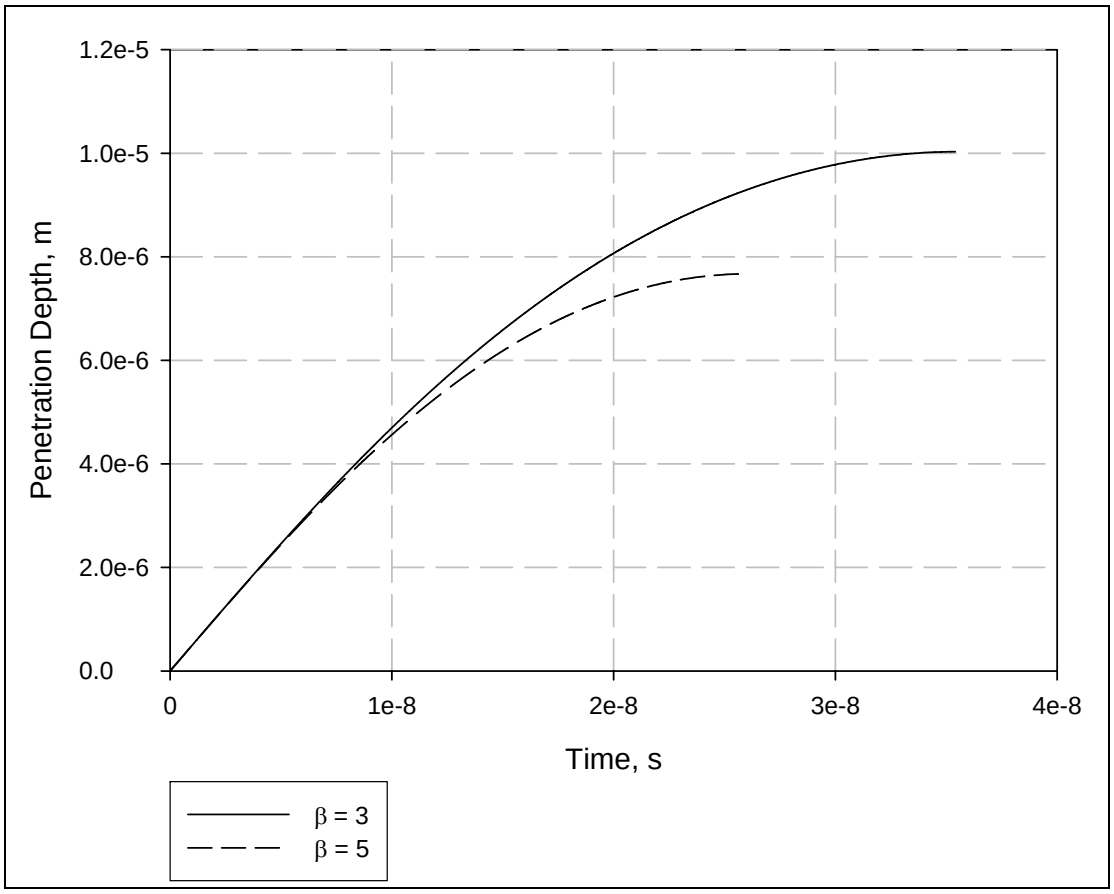

Figure 3. Calculated penetration vs. time for 22-μm copper particles impacting 304 stainless at 500-m/s steel for two values of β.

values of β equal to 3 and 5, respectively. This equates to a normalized penetration depth, X/R, of 0.91 and 0.70 for values of β equal to 3 and 5, respectively. From the experiments, X/R = 0.3, so that there is a large difference between the model results and the observations. This disparity is most likely attributable to the rigid body assumption.

Several attempts were made to include particle deformation effects in a more complicated model that did not use the rigid body assumption. These attempts did no better in producing a model that could be used to estimate the value of X/R accurately.

Frank and Zook (*16*) have modified equation 5 for the noneroding rod penetrator case (u = v) and added a term that accounts for unsteady motion (*8, 10*):

$$Y_p = k_t \rho_t v^2 + R_t + k_1 \rho_t D \, dv/dt \, . \qquad (14)$$

Here, k_t and k_1 are fitting parameters, and D is the penetrator diameter. (Note that k_t takes the place of 1/2 in equation 5.) Define the rate of penetration as dx/dt = v. The penetrator is decelerated according to equation 15:

$$dv/dt = - Y_p/L\rho_p, \qquad (15)$$

where L is the penetrator length. Equations 14 and 15 can be solved to obtain

$$X/R = ((L/D\ \rho_p/\rho_t + k_1)/2kt)\ln(1+k_t\rho_t V^2/R_t). \quad (16)$$

In this equation, V is the impact velocity. Frank and Zook (*16*) fit high-density, low-L/D-ratio penetrator data to equation 16 to obtain the following values of the fitting parameters and R_t:

$$k_1 = 0.557,$$
$$k_t = 1.046,$$
$$R_t = 9.13 \times 10^9 \text{ Pa}. \quad (17)$$

Here, R_t is the target resistance value for rolled homogeneous (steel) armor (RHA). The authors recognized that the value of the target resistance was about twice that ordinarily used for eroding long rod penetrators. They suggested that the energy lost in deforming the penetrator (but not eroding it) was responsible for this increase in apparent target resistance.

The Frank-Zook formulation can be used to make a first estimate of copper sphere impact depths into stainless steel. First, assume that a sphere is the mass equivalent of a cylinder with L/D = 1. Therefore, the L/D ratio for the sphere equivalent is 2/3. Next, substitute the appropriate density values in equation 16 and use the parameters listed in equation 17. This produces a value of 0.278 for X/R. This value is slightly less than that obtained with the analysis in section 2. The data that Frank and Zook used to fit their equation involved impacts into steel RHA. Therefore, the strength difference between RHA and stainless steel might account for some of the difference. If the value of 7.6×10^9 Pa is used for R_t, then equation 16 gives 0.297 for X/R.

The Frank-Zook formulation suffers from the same drawback as other approaches. That is, the target resistance cannot be determined *a priori* from first principles. Consequently, it cannot make independent predictions for low-velocity impacts of a variety of material combinations. It is interesting to note that this approach comes closer to the result determined from the data analysis than the other approaches tested. This may be fortuitous, considering the material properties and small size of the impacting particles.

4. Discussion

A one-dimensional penetration model has been adapted to the case of a copper particle impacting stainless steel at 500 m/s. A rigid body assumption was used to enable the calculations to be carried out. It is not surprising, therefore, that the calculated penetration depth is not in good agreement with experimental observations. The normalized penetration depths derived from the model are over two times too high (0.9 or 0.7 vs. 0.3).

As a point of comparison, a standard penetration mechanics code (Autodyne*) was used for the same calculation. The values of the copper and steel yield stress that were used for the calculation were 120 and 300 MPa, respectively. For reasons already mentioned, these values may not be appropriate for this calculation. In addition, the version of Autodyne that was used for these calculations cannot formulate its cells with a length scale smaller than 1 mm. Therefore, it was assumed that in the absence of any rate-dependent material properties scaling would be valid. The calculations were carried out for a spherical copper particle 10 mm in diameter. A plot of the penetration depth, normalized by the original radius, is shown in figure 4. The final normalized penetration depth (X/R) fluctuated around 0.52 for times greater than 40 μs.

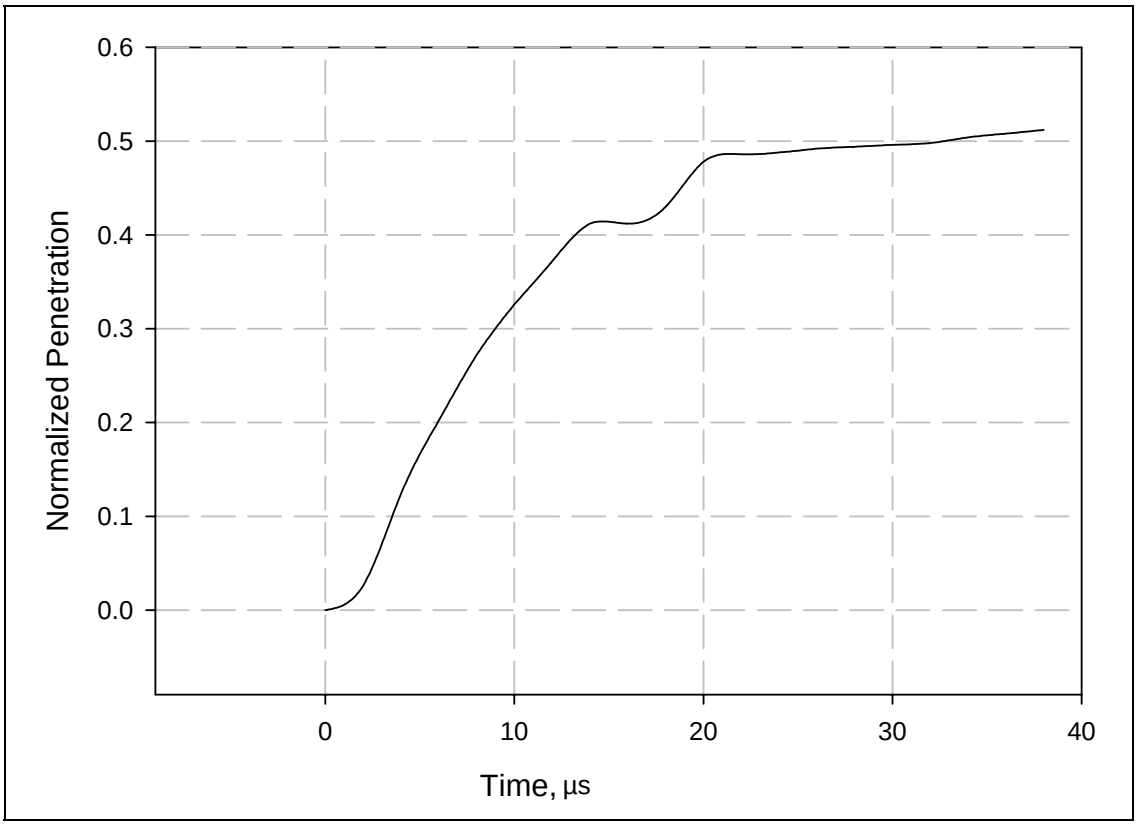

Figure 4. Autodyne calculation of normalized penetration depth (X/R) vs. time; 10-mm diameter copper sphere impacting stainless steel at 500 m/s.

In addition, measurements taken from the figures generated by the CTH code in Dykhuizen et al. (*1*) showed a normalized penetration depth of 0.41 for a 25-μm copper particle impact on stainless steel for an impact velocity of 500 m/s. The CTH code takes into account such effects as the pressure dependence of the yield strength and strain hardening. It predicts impact pressures up to 5 GPa for this calculation. Thus, predictions from more sophisticated codes also over-estimate the depth of penetration.

* Autodyne is a registered trademark of the Ansys Corporation.

Several possible causes for the over-estimation can be offered. First, all the approaches assume that the copper particles are perfectly spherical at impact. If they are not perfectly spherical and hit the target with a flat surface, then the penetration depth will decrease. This is because they have a relatively larger contact surface from the beginning of the calculation.

One other source of error is the neglect of any elastic rebound. An effect called "shallowing" has been observed in many cases of static indentation (*17*). When an indenter (e.g., Brinnell hardness ball) is lifted from the surface of a sample after having made an indentation, it is observed that the indentation has a larger radius of curvature than the indenting ball. That is, the indentation depth achieved by the ball is not retained but relaxes to a lower value. Because of the shallowing effect, depth measurements are unreliable and are not used in the hardness determination. Such an elastic relaxation may have occurred in the work reported by Dykhuizen et al. (*1*) as a result of removing the copper particles from the stainless steel.

The model has been pursued assuming that averages of experimental parameters are appropriate for comparing with model predictions. In particular, we have used an average particle size traveling at an average velocity for the calculations. It may be that for any given spraying operation, the smaller particles travel faster than the larger ones and produce deeper craters in relation to their diameters (see figure 1). As previously mentioned, there is a range of particle velocities in any given particle stream. (The particle velocity distribution approximates a Gaussian distribution with about a 50-m/s mean deviation.) If the average velocity of the stream is low, then only the smaller, faster particles will adhere. As the average particle velocity increases, larger particles will have sufficient velocity to adhere to the target and deposition efficiency will increase. It is the slower particles in the stream that will produce the incipient conditions for particle sticking for elevated average particle velocities. Model calculations showed that the value of X/R for different size particles was the same.

However, the model does predict that effect of particle velocity on X/R is more pronounced. The velocity was varied from 400 to 500 m/s, and the results are presented in figure 5. A particle radius of 11 μm and a $\beta = 5$ were used for the calculations. Dykhuizen et al. (*1*) did not observe any particle sticking at an average particle velocity of 400 m/s. If there were any particles in this stream with a velocity of 450 m/s, they did not adhere or were too few in number to be observed. Particle adhesion was observed for an average particle velocity of 521 m/s. However, the deposition efficiency was low at this velocity, suggesting that only faster-than-average particles were adhering. Therefore, velocity distribution effects cannot explain the difference between the model predictions and observed penetration depths.

One final point can be made regarding the target resistance. If the target experiences a strain rate similar to that experienced by the particle, then it would be reasonable to assume that the target resistance would also increase. This would lead to a smaller depth of penetration.

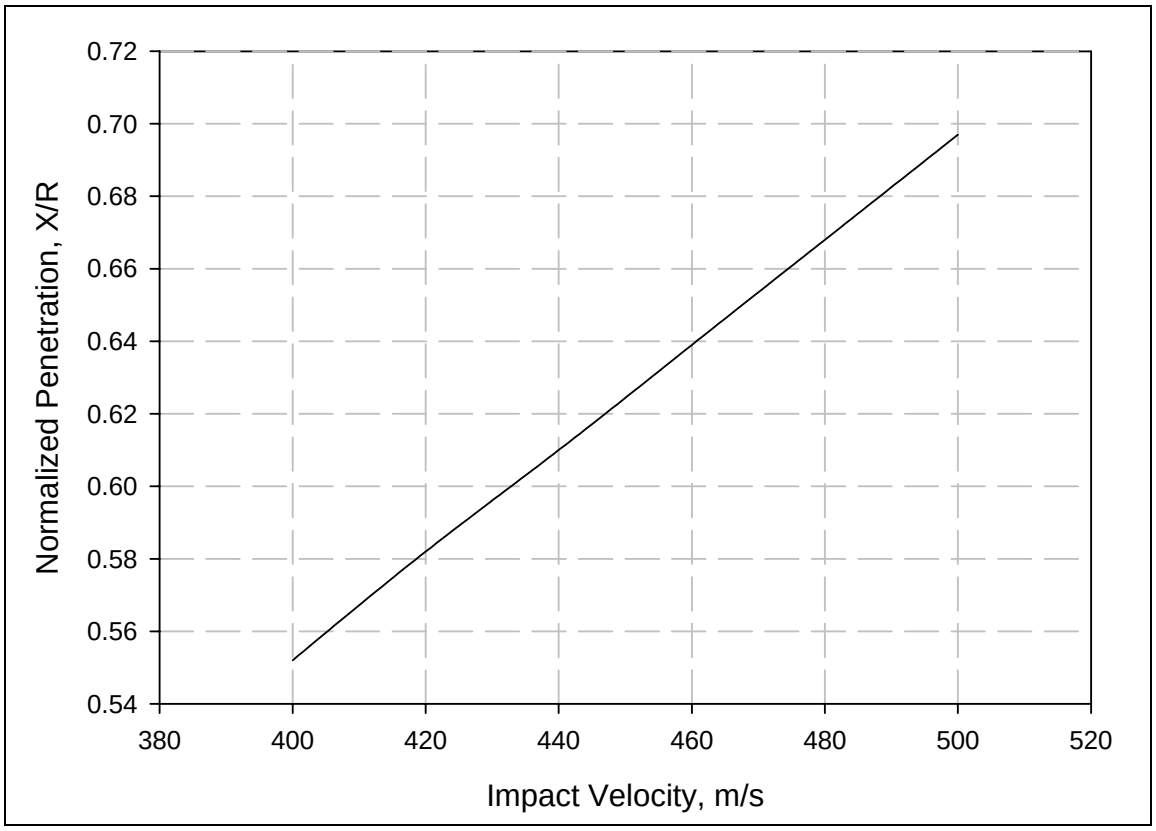

Figure 5. Normalized penetration vs. impact velocity (model calculation).

5. General Comments

At the outset of this work, it was anticipated that a model could be developed that would be able to predict accurately the value of X/R for a range of material combinations. However, the goal of developing an accurate model was not achieved. This is due in large part of the unknown material properties of both the target and particle material in the scale of sizes and strain rates pertinent to cold spray. In addition, the possibility that there exists a single minimum value of X/R for all material combinations that would assure particle adherence is unlikely, given the wide range of material properties.

One of the most intriguing points brought out by the analysis of the cold-spray impact data is that particle sticking can occur for low penetration depths. Analysis of data involving copper particles sprayed onto a 304 stainless steel target indicate that the normalized penetration depth, X/R, is ~0.3. That is, a copper particle needs only to be buried less than a third of its radius (one-sixth of the diameter) for adhesion to take place on stainless steel. Certainly, at a very high

velocity that produces deep penetration of the target, there is a strong frictional and/or mechanical bond that welds the particle to the substrate. How and to what extent incipient bonding occurs is not so clear.

One possibility for a frictional or mechanical bond is presented in figure 6, which shows a stylized and somewhat exaggerated cross-section of the edge of a crater and the shape of the deformed particle. Here, a shallow crater has been formed, and material has been ejected from the crater to form a lip. At some later time, the particle has ceased to penetrate the target. However, it is assumed that the rear of the particle continues to deform and be decelerated until it comes to rest, encompassing, to some extent, the crater lip. This drawing is not unlike the actual crater and particle formation shown in figure 8 of Dykhuizen et al. (*1*). However, the cross-section shown in Dykhuizen, et al. appears to lack any mechanical interference that would be the source of bonding. This lack of detail is not surprising, considering the small scale of the cross-section.

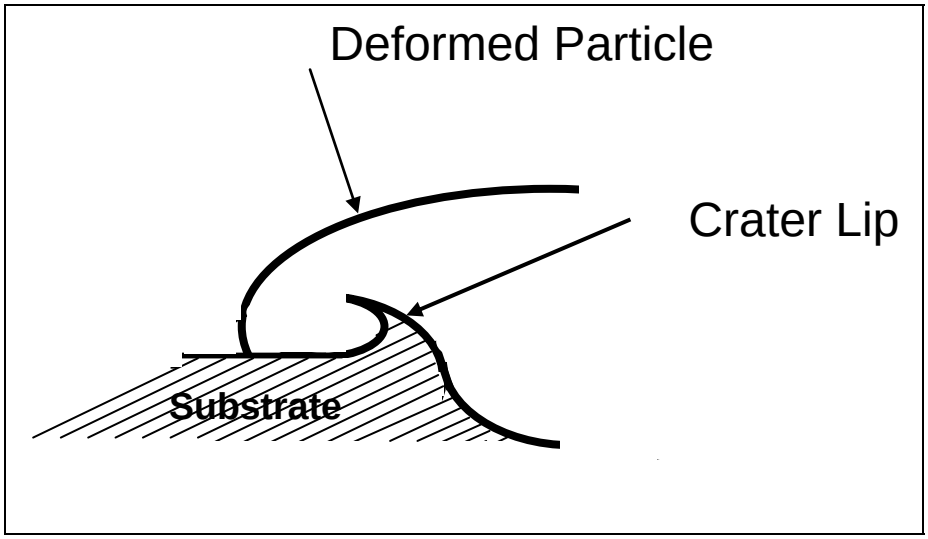

Figure 6. Exaggerated picture of incipient bonding mechanism showing cross section of crater lip and deformed particle.

The bonding mechanism pictured in figure 6 may be unique to the copper-stainless steel combination of materials, or other material combinations with densities and material strengths that are similar. Consider next a very hard material impacting a soft substrate, such as tungsten particles impacting annealed aluminum. In this case, the bonding may occur as a result of embedment of the particle in the substrate, giving a high value of the normalized penetration depth. The bond would depend to some extent on friction and elastic recompression of the substrate material. A possible representation of this bonding mechanism is shown in figure 7. The value of X/R for this figure is a little over one; this value might be different for different material combinations. Note that the impact velocity for actually building up a thick layer of tungsten may be substantially different from the value needed for initial adhesion. Finally, there

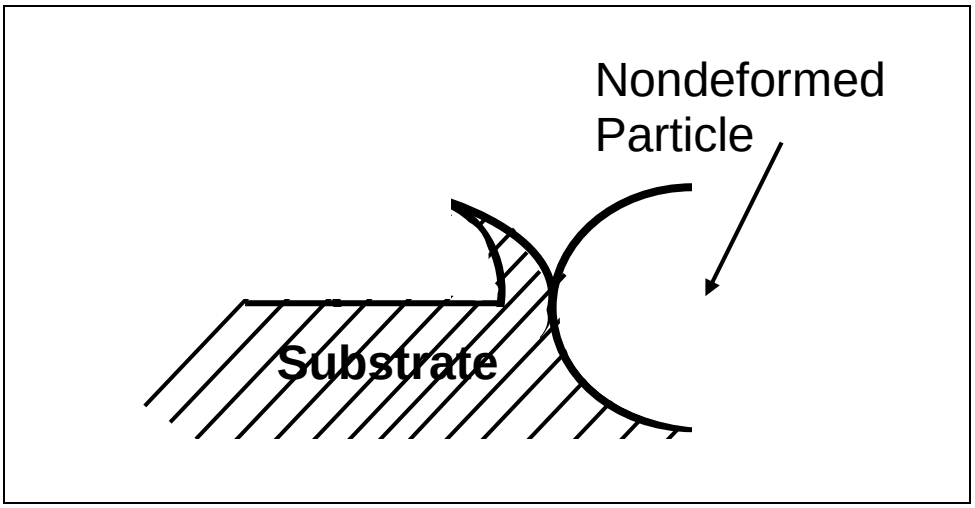

Figure 7. Incipient bonding mechanism (frictional/mechanical) for nondeformed particle.

is the case where the particle strength is much less than that of the substrate. Unless the density of the particle is high enough to make a crater (i.e., the ρu^2 term is large), then a mechanical bond might not be possible.

6. Summary

It is widely accepted that for any given combination of particle and substrate used in the cold-gas dynamic spray process, there is a minimum impact velocity required to achieve particle adhesion. A first hypothesis was that there might exist a normalized penetration depth, X/R, that would provide adhesion for all material combinations. If this were the case, then some insight might be gained as to the nature of the bond between the particle and substrate. To test this hypothesis, a one-dimensional model was developed to describe the penetration process. In addition, published data on the impact of penetration of copper particles onto a 304 stainless steel substrate have been analyzed to estimate the value of X/R when adhesion first begins. From these data, the critical normalized penetration depth was determined to be ~0.3 for this particular particle-substrate combination. The one-dimensional model developed here was found not to agree well with the observed results. Computer code results from CTH and Autodyne were also found to over-estimate the observed penetration depths. Several possible explanations for the discrepancy were discussed. The primary problem centers around the unknown material properties at the strain rates and scale sizes pertinent to cold spray. Another plausible explanation is that there was some elastic relaxation of the material in the crater after the copper particle was removed, leading to a decrease in the observed penetration depth. Mechanical bonding was suggested as the primary mechanism for particle adhesion. The exact nature of this process would depend on the relative flow properties and densities of the particle and substrate materials.

7. References

1. Dykhuizen, R. C.; Smith, M. F.; Gilmore, D. L.; Neiser, R. A.; Jiang, X.; Sampath, S. Impact of High Velocity Cold Spray Particles. *Journal of Spray Technology* **1999**, *8* (4).

2. Grujicic, M.; Zhao, C. L.; de Rosset, W. S.; Helfritch, D. Adiabatic Shear Instability Based Mechanism for Particle/Substrate Bonding in the Cold-Gas Dynamic-Spray Process. *Materials and Design* **2004**, *25* (8).

3. Hammad, A.; Gartner, F.; Stoltenhoff, T.; Kreye, H. Bonding Mechanism in Cold Gas Spraying. *Acta Materialia* **2003**, *51*.

4. Grujicic, M.; Saylor, J. R.; Beasley, D. E.; de Rosset, W. S.; Helfritch, D. Computational Analysis of the Interfacial Bonding Between Feed Particles and the Substrate in the Cold-Gas Dynamic Spray Process. *Applied Surface Science* **2003**, *219*, 211–237.

5. Dykhuizen, R. C.; Smith, M. F. Gas Dynamic Principles of Cold Spray. *Journal of Thermal Spray Technology* **1998**, *7* (2).

6. Smith, M. F.; Brockman, J. E.; Dykhuizen, R. C.; Gilmore, D. L.; Neiser, R. A.; Roemer, T. J. Cold Spray Direct Fabrication – High Rate, Solid State, Material Consolidation. *Proceedings of the Fall 1998 Meeting of the Materials Research Society*, Boston, MA, 30 November–4 December 1998.

7. Tate, A. A Theory for the Deceleration of Long Rods After Impact. *J. Mech. Phys. Solids* **1967**, *15*, 387–399.

8. Tate, A. Further Results in the Theory of Long Rod Penetration. *J. Mech. Phys. Solids* **1969**, *17*, 141–150.

9. Alekseevskii, V. P. *Penetration of a Rod Into a Target at High Velocity, in Combustion, Explosion and Shock Waves*, Faraday Press: New York (translated from Russian), 1966; Vol. 2, pp 63–66.

10. Goodier, J. N. On the Mechanics of Indentation and Cratering in Solid Targets of Strain-Hardening Metal by Impact of Hard and Soft Spheres. *Proceedings of the Seventh Hypervelocity Impact Symposium*, Vol. III, Martin Company, Tampa, FL, 1965.

11. Walker, J. D.; Anderson, C. E., Jr. A Time-Dependent Model for Long Rod Penetration. *Int. J. Impact Engng.* **1995**, *16*, 19–48.

12. Florence, A. L.; Gefken, P. R.; Kirkpatrick, S. W. Dynamic Plastic Buckling of Copper Cylindrical Shells. *Int. J. Solids Structures* **1991**, *27* (1), 89–103.

13. Pepi, M. U.S. Army Research Laboratory, Aberdeen Proving Ground, MD. Private communication, 21 February 2006.

14. Segletes, S. B. *Analysis of the Noneroding Penetration of Tungsten Alloy Long Rods Into Aluminum Targets*; ARL-TR-3075; U.S. Army Research Laboratory: Aberdeen Proving Ground, MD, September 2003.

15. Segletes, S. B. *Analysis of Erosion Transition in Tungsten-Alloy Long Rods Into Aluminum Targets*; ARL-TR-3153; U.S. Army Research Laboratory: Aberdeen Proving Ground, MD, March 2004.

16. Frank, K.; Zook, J. Chunky Metal Penetrators Act Like Constant Mass Penetrators. *In Proceedings of the 12th International Symposium on Ballistics*, San Antonio, TX, 30 October–1 November 1990; Vol. 1, pp 441–449.

17. Tabor, D. *The Hardness of Metals*; Oxford at the Clarendon Press: London, E.C.4, 1951.

Appendix. Calculation Procedure

The force law is assumed to be given by

$$\Sigma (\pi a^2) = (\tfrac{1}{2} \rho_t u^2 + R_t) \pi a^2 , \qquad \text{(A-1)}$$

where a is the radius of the contact area, ρ_t is the target density, u is the penetration velocity, and R_t is the target resistance. The target resistance is assumed to take the form

$$R_t = \beta Y_t , \qquad \text{(A-2)}$$

where Y_t is the target yield strength and β is a constant of proportionality.

The contact area, πa^2, is calculated from

$$\pi a^2 = \pi(Dx - x^2), \qquad \text{(A-3)}$$

where D is the particle diameter and x(t) is the coordinate of the center of mass. The initial conditions are that the center-of-mass velocity is the impact velocity, the center of mass os located at the origin. The calculation is done in 0.2-ns intervals. For the first time step, x is approximated by multiplying the center-of-mass velocity by 0.1 ns. This gives the mid-point value of x for the time interval of 0.2 ns. The value of the acceleration is then calculated. This mid-point approximation of the acceleration is then used to calculate the velocity at the end of the time interval. This velocity is the initial velocity for the next time interval. The same procedure is repeated for the next time step, except that the time interval now is the entire 0.2 ns. The calculation is continued until the center-of-mass velocity is less than 1 m/s. The first few time steps are shown below.

Table A-1. Rigid body penetration.

R =	1.10E-05				
Density =	8.90E+03				
M =	4.96E-11				
D =	2.20E-05				
Initial vel =	500				
Rt =	3.50E+09				
Time		**dx/dt initial**	**x**	**d^2x/dt^2**	**dx/dt final**
0		500	0	0	
2.00E-10		500	5.00E–08	3.11E+08	5.00E+02
4.00E-10		5.00E+02	1.50E–07	9.30E+08	5.00E+02
6E-10		5.00E+02	2.50E–07	1.54E+09	4.99E+02
8.00E-10		4.99E+02	3.50E–07	2.15E+09	4.99E+02

NO. OF COPIES	ORGANIZATION
1 (PDF ONLY)	DEFENSE TECHNICAL INFORMATION CTR DTIC OCA 8725 JOHN J KINGMAN RD STE 0944 FORT BELVOIR VA 22060-6218
1	US ARMY RSRCH DEV & ENGRG CMD SYSTEMS OF SYSTEMS INTEGRATION AMSRD SS T 6000 6TH ST STE 100 FORT BELVOIR VA 22060-5608
1	DIRECTOR US ARMY RESEARCH LAB IMNE ALC IMS 2800 POWDER MILL RD ADELPHI MD 20783-1197
3	DIRECTOR US ARMY RESEARCH LAB AMSRD ARL CI OK TL 2800 POWDER MILL RD ADELPHI MD 20783-1197

ABERDEEN PROVING GROUND

1	DIR USARL AMSRD ARL CI OK TP (BLDG 4600)

NO. OF COPIES ORGANIZATION

1 DIRECTOR
US ARMY RESEARCH LAB
AMSRD ARL SE DE
R ATKINSON
2800 POWDER MILL RD
ADELPHI MD 20783-1197

5 DIRECTOR
US ARMY RESEARCH LAB
AMSRD ARL WM MB
A ABRAHAMIAN
M BERMAN
M CHOWDHURY
T LI
E SZYMANSKI
2800 POWDER MILL RD
ADELPHI MD 20783-1197

1 COMMANDER
US ARMY MATERIEL CMD
AMXMI INT
9301 CHAPEK RD
FORT BELVOIR VA 22060-5527

2 PM MAS
SFAE AMO MAS MC
PICATINNY ARSENAL NJ
07806-5000

1 US ARMY ARDEC
SFAE AMO MAS LC
D RIGOGLIOSO
BLDG 354 M829E3 IPT
PICATINNY ARSENAL NJ
07806-5000

1 DIRECTOR
AIR FORCE RESEARCH LAB
MLLMD
D MIRACLE
2230 TENTH ST
WRIGHT PATTERSON AFB OH
45433-7817

1 OFC OF NAVAL RESEARCH
J CHRISTODOULOU
ONR CODE 332
800 N QUINCY ST
ARLINGTON VA 22217-5600

NO. OF COPIES ORGANIZATION

1 PM MAS
SFAE AMO MAS
CHIEF ENGINEER
PICATINNY ARSENAL NJ
07806-5000

1 COMMANDER
US ARMY TACOM
AMSTA SF
WARREN MI 48397-5000

1 COMMANDER
WATERVLIET ARSENAL
SMCWV QAE Q
B VANINA
BLDG 44
WATERVLIET NY 12189-4050

2 COMMANDER
US ARMY AMCOM
AVIATION APPLIED TECH DIR
J SCHUCK
FORT EUSTIS VA 23604-5577

1 US ARMY TARDEC
AMSRD TAR R
D TEMPLETON
6501 E 11 MILE RD MS 263
WARREN MI 48397-5000

14 BENET LABS
AMSTA AR CCB
R FISCELLA
M SOJA
E KATHE
M SCAVULO
G SPENCER
P WHEELER
S KRUPSKI
J VASILAKIS
G FRIAR
R HASENBEIN
AMSTA CCB R
S SOPOK
E HYLAND
D CRAYON
R DILLON
WATERVLIET NY 12189-4050

NO. OF COPIES	ORGANIZATION
1	NSWC TECH LIBRARY CODE B60 17320 DAHLGREN RD DAHLGREN VA 22448
7	US ARMY RESEARCH OFC A CROWSON H EVERITT J PRATER G ANDERSON D STEPP D KISEROW D SKATRUD PO BOX 12211 RESEARCH TRIANGLE PARK NC 27709-2211
2	DARPA S WAX L CHRISTODOULOU 3701 N FAIRFAX DR ARLINGTON VA 22203-1714
1	DIRECTOR NGIC IANG TMT 2055 BOULDERS RD CHARLOTTESVILLE VA 22911-8318
3	PACIFIC NORTHWEST LAB M SMITH G VAN ARSDALE R SHIPPELL PO BOX 999 RICHLAND WA 99352
1	ZERNOW TECHNICAL SERVICES L ZERNOW 425 W BONITA AVE STE 208 SAN DIMAS CA 91773
2	GENERAL DYNAMICS OTS FLINCHBAUGH DIV K LINDE T LYNCH PO BOX 127 RED LION PA 17356
1	GDLS DIVISION D BARTLE PO BOX 1901 WARREN MI 48090

NO. OF COPIES	ORGANIZATION
5	INST FOR ADVANCED TECH H FAIR I MCNAB P SULLIVAN S BLESS C PERSAD 3925 W BRAKER LN AUSTIN TX 78759-5316
1	R EICHELBERGER CONSULTANT 409 W CATHERINE ST BEL AIR MD 21014-3613
1	JOHNS HOPKINS UNIV APPLIED PHYSICS LAB P WIENHOLD 11100 JOHNS HOPKINS RD LAUREL MD 20723-6099
5	UNIV OF DELAWARE CTR FOR COMPOSITE MTRLS J GILLESPIE M SANTARE S YARLAGADDA S ADVANI D HEIDER 201 SPENCER LAB NEWARK DE 19716
1	DEPT OF MTRLS SCIENCE & ENGRG UNIV OF ILLINOIS AT URBANA CHAMPAIGN J ECONOMY 1304 W GREEN ST 115B URBANA IL 61801
1	SOUTHWEST RESEARCH INST ENGR & MATL SCIENCES DIV J RIEGEL 6220 CULEBRA RD PO DRAWER 28510 SAN ANTONIO TX 78228-0510
3	DIRECTOR US ARMY RESEARCH LAB AMSRD ARL WM MB A FRYDMAN 2800 POWDER MILL RD ADELPHI MD 20783-1197

NO. OF COPIES ORGANIZATION

1 DEPARTMENT HEAD
US MILITARY ACADEMY
K NYGREN
CIVIL & MECH ENGRG DEPT
WEST POINT NY 10996-1792

1 DIRECTOR
US MILITARY ACADEMY
D BOETTNER
MECH ENGRG DIV
WEST POINT NY 10996-1792

1 US ARMY ARDEC
AMSTA AR FSA
A WARNASH
BLDG 1
PICATINNY ARSENAL NJ
07806-5000

1 US ARMY ARDEC
AMSRD AAR ATD B
B MACHAK
BLDG 1
PICATINNY ARSENAL NJ
07806-5000

1 US ARMY ARDEC
AMSTA AR FSP G
D CARLUCCI
BLDG 1
PICATINNY ARSENAL NJ
07806-5000

ABERDEEN PROVING GROUND

1 US ARMY ATC
CSTE DTC AT AD I
W C FRAZER
400 COLLERAN RD
APG MD 21005-5059

58 DIR USARL
AMSRD ARL CI
AMSRD ARL O AP EG
M ADAMSON
AMSRD ARL SL BM
D BELY
AMSRD ARL WM B
CHIEF
AMSRD ARL WM BC
J NEWILL
P PLOSTINS
AMSRD ARL WM BD
P CONROY
B FORCH
AMSRD ARL WM BF
S WILKERSON
AMSRD ARL WM M
J MCCAULEY
S MCKNIGHT
AMSRD ARL WM MA
CHIEF
AMSRD ARL WM MB
J BENDER
T BOGETTI
L BURTON
R CARTER
K CHO
W DE ROSSET
R DOWDING
W DRYSDALE
R EMERSON
D GRAY
D HOPKINS
R KASTE
L KECSKES
M MINNICINO
B POWERS
D SNOHA
J SOUTH
M STAKER
J SWAB
J TZENG
AMSRD ARL WM MC
CHIEF
V CHAMPAGNE
S GRENDAHL
M PEPI
D HELFRITCH
W SPURGEON
AMSRD ARL WM MD
B CHEESEMAN
E CHIN
P DEHMER
R DOOLEY
C FOUNTZOULAS
G GAZONAS
J MONTGOMERY
B SCOTT

NO. OF
COPIES ORGANIZATION

AMSRD ARL WM TA
M BURKINS
B GOOCH
T HAVEL
C HOPPEL
E HORWATH
J RUNYEON
AMSRD ARL WM TB
P BAKER
AMSRD ARL WM TC
R COATES
AMSRD ARL WM TD
D DANDEKAR
M RAFTENBERG
S SEGLETES
T WEERASOORIYA

NO. OF COPIES ORGANIZATION

1 DRA FORT HALSTEAD
P N JONES
SEVEN OAKS KENT TN 147BP
UK

1 SWISS FEDERAL ARMAMENTS WKS
W LANZ
ALLMENDSTRASSE 86
3602 THUN
SWITZERLAND

1 DYNAMEC RESEARCH LAB
AKE PERSSON
BOX 201
SE 151 23 SODERTALJE
SWEDEN

1 ISRAEL INST OF TECHLGY
S BODNER
FACULTY OF MECHANICAL ENGR
HAIFA 3200
ISRAEL

1 DSTO
WEAPONS SYSTEMS DIVISION
N BURMAN RLLWS
SALISBURY
SOUTH AUSTRALIA 5108
AUSTRALIA

1 DEF RES ESTABLISHMENT VALCARTIER
A DUPUIS
2459 BLVD PIE XI NORTH
VALCARTIER QUEBEC
CANADA
PO BOX 8800 COURCELETTE
GOA IRO QUEBEC
CANADA

1 TNO DEFENSE SECURITY & SAFETY
R R IJSSELSTEIN
PO BOX G6S64
D HAAS
2509 JG
THE NETHERLANDS

NO. OF COPIES ORGANIZATION

2 FOA NATL DEFENSE RESEARCH ESTAB
DIR DEPT OF WEAPONS & PROTECTION
B JANZON
R HOLMLIN
S 172 90 STOCKHOLM
SWEDEN

1 DEUTSCHE AEROSPACE AG
DYNAMICS SYSTEMS
M HELD
PO BOX 1340
D 86523 SCHROBENHAUSEN
GERMANY

INTENTIONALLY LEFT BLANK.